# Graphite-Based Multianalyte VOC Gas Detection on Multichannel PCB IDE Sensor

João Paulo de Campos da Costa, *Member, IEEE*, Leonélio Cichetto Junior, Estácio Paiva de Araújo, Adryelle do Nascimento Arantes, Elson Longo, Adenilson José Chiquito, and João Paulo Carmo

***Abstract*—In this article, we present the development of a volatile organic compound (VOC) gas sensor based on graphite on a printed circuit board (PCB) multiplexed interdigitated electrode (IDE) sensor. We report the effects of graphite as a sensing material deposited by the spray method and its interaction response to specific gases. In addition, we demonstrate how we designed and manufactured IDE sensors with an integrated heating circuit and thermistor element, as well as the 55-$\mu$L microchamber, which contributed to the fast detection of gases. All experiments were performed with four IDE sensors to verify the reproducibility and sensitivity of the proposed methodology. Our results highlight that acetone presented the highest detection sensitivity, with an electric current increase of ±100 $\mu$A at a 200-ppm cycle with a response of 0.92 s and full recovery at 2.62 s. Furthermore, the developed sensors were able to detect and distinguish between acetone, methanol, isopropanol, ethanol, and chloroform gases. The sensors exhibited outstanding stability and repeatability when evaluated after six months. The sensors' operation at 2 V makes it suitable for low-power devices with a high potential to be applied in future commercial room-temperature VOC gas sensor devices.**

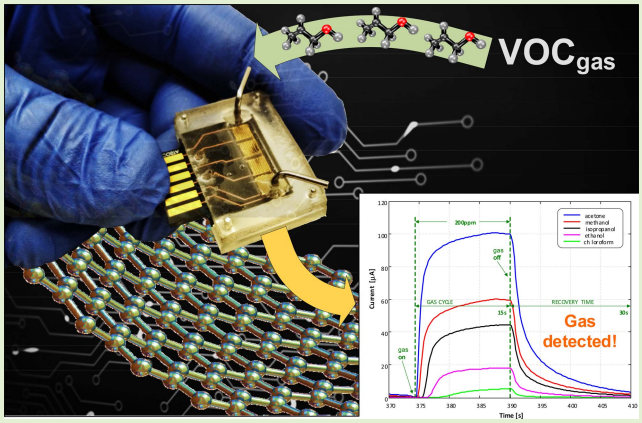


***Index Terms*—Gas sensor, graphite, multiplexed detection, volatile organic compounds.**

## I. Introduction

OVER the last few years, a substantial increase in gas emission has driven the development of highly sensitive and selective gas sensors able to detect low concentrations (part per million, ppm) of polluting, flammable, and hazardous gases [1], [2], [3], [4], [5], [6], [7], [8], [9], [10]. In particular, toxic gases composed of volatile organic compounds (VOCs) tend to be of interest to the sectors of medicine, automotive, and oil industries for monitoring and preventing individual exposure [11], [12], [13], [14], [15].

Regarding gas-sensing electronic devices, several materials as sensing active layers have been reported, and among them, when low concentration detection is required, semiconductor materials and metallic oxides are commonly employed [16]. However, it remains a challenge to ensure their reproducibility, sensitivity, selectivity, room temperature operability, and low manufacturing costs for commercial applications [17], [18].

Recent studies have shown that sensor materials based on $sp^2$-type carbon structures, such as graphene, graphene oxide, reduced graphene, and carbon nanotubes, are promising candidates for the development of highly sensitive, low-cost, and highly selective gas sensors for room-temperature applications, due to their physical–chemical properties, such as high conductivity, chemical, and thermal stability [19], [20], [21], [22]. Nevertheless, graphite-based devices have hardly been reported, which became this work's main motivation.

Anjum et al. [23] have presented a method for detecting alcoholic vapors individually and in mixture forms through

Manuscript received 23 August 2022; accepted 23 September 2022. Date of publication 3 October 2022; date of current version 14 November 2022. This work was supported in part by the Grant Centros de Pesquisa, Inovação e Difusão (CEPID)/Centro de Desenvolvimento de Materiais Funcionais (CDMF)—São Paulo Research Foundation—Fundação de Amparo á Pesquisa do Estado de São Paulo (FAPESP) under Grant 2013/07296-2, Grant 2014/01371-5, Grant 2017/23663-6, and Grant 2019/18656-6; and in part by Conselho Nacional de Desenvolvimento Científico e Tecnológico (CNPq) under Grant 305656/2018-0 and Grant 304312/2020-7. The associate editor coordinating the review of this article and approving it for publication was Dr. Yang Yang. *(Corresponding author: João Paulo de Campos da Costa.)*

João Paulo de Campos da Costa and João Paulo Carmo are with the Department of Electrical Engineering (SEL), University of São Paulo (USP), São Paulo, São Carlos 13566-590, Brazil (e-mail: joaoccosta@usp.br).

Leonélio Cichetto Junior, Estácio Paiva de Araújo, Adryelle do Nascimento Arantes, and Adenilson José Chiquito are with the Physical Department–NanOLaB, Federal University of São Carlos (UFSCar), São Paulo, São Carlos 13565-905, Brazil.

Elson Longo is with INCTMN-CDMF, Department of Chemistry, Federal University of São Carlos (UFSCar), São Paulo, São Carlos 13565-905, Brazil.

Digital Object Identifier 10.1109/JSEN.2022.3210007

the use of graphite-doped calcium hydroxyapatite nanoceramic materials. The sensors showed optimal performance at temperatures between 30 °C and 60 °C, for a gas concentration of 100 ppm, with a range of responses from 100% to 460% for different gases, and rise and recovery times between 60 and 200 s [23]. Yu et al. [24] reported porous $\alpha$-$Fe_2O_3$ nanorod graphite nanocomposites, which displayed a high sensitivity of 16.9 toward 50-ppm acetone at an operating temperature of 260 °C. Sakar Dasdan [25] presented an interdigitated electrode (IDE) fabricated by drop casting of graphite-loaded poly(phenyl sulfone) (PPSU/Gr) film on a conductive substrate. IDE sensors were experimentally tested at room temperature, and their sensitivity ranged from 10% to 90% for different solvents, under saturated pressure [25]. More recently, Wang et al. [26] described the fabrication of a self-powered flexible gas sensor based on MXene/Ag with high sensitivity to ethanol (204% at 100 ppm) at room temperature, which is 24.5 times higher than resistive gas sensors.

As an attempt to overcome some of the previously mentioned challenges regarding the development of reliable gas-sensing devices, we demonstrate the design and fabrication of a four-electrode multiplexed IDE sensor using graphite as a sensing layer, built by a spray deposition method, with a microchamber structure, operating at room temperature. We discuss the gas-sensing properties of graphite employed as a VOC gas detector, considering acetone, methanol, isopropanol, ethanol, and chloroform. The electrical characterization methods with and without the presence of each studied VOC gas selected were the current over time ($I$–$t$) curves and current over concentration.

## II. Background

The fundamental working principle of gas sensors is based on conductivity parameter alteration, for example, resistance [Ω], electric current [A], frequency [Hz], and conductance [G], when exposed to different gas concentrations. To carry out the studies and acquire signals generated by adsorption/desorption processes on the active layer, impedance spectroscopy, resistance over time, conductometry, and current over time techniques (chronoamperometry) are commonly employed.

Chronoamperometry (CA) has been highlighted as an important technique applied for gas sensor signal acquisition due to its high sensitivity, ease of circuit design and fabrication, low cost, as well as reduced components for the instrumentation. This technique can be used to track changes in current over time through a potentiostat/galvanostat circuit, responsible for keeping a constant voltage while recording the current generated by faradaic processes between two electrodes [27], [28]. The faradaic current generated from these reactions can be used to determine the concentration of the gas being detected as well as its specificity. The sensor's sensitivity can be estimated based on its conductivity response $X$, when exposed to ambient air or by an inert gas ($N_2$), in relation to the conductivity response to a particular analyzed gas concentration[29], for example,

$$\text{Sensitivity } (S) = \frac{X_{\text{gas}} - X_{N_2}}{X_{N_2}}. \quad (1)$$

The selectivity of the sensor is determined by comparing the conductivity values of the sensor when exposed to different gases with different concentrations, and the reversibility performance is evaluated by comparing the recovery time(s) after gas exposure after several cycles [29].

## III. Experiment

The IDEs were designed using ECAD software (Proteus LabCenter) and manufactured using LPKF ProtoMat S63 on a double-sided, 2-oz-thick copper-clad printed circuit board (PCB) substrate FR4 (model Kingboard KB6167F). The substrate was selected due to its electrical, mechanical, and chemical properties, which remain stable up to 175 °C. The circuits of the sensor were coated with gold by a chemical process (ENIG, according to IPC-4552) to improve the high corrosion resistance and ensure the reproducibility of the developed sensor for gas experiments. The electrical connections are protected by a black resin solder mask.

Fig. 1(a) shows a schematic of the multichannel sensor with the sensing circuit on the top side and the heating circuit on the bottom side of the PCB substrate. The integrated heater circuit was designed to ensure optimum performance when using sensing materials that require an increase in temperature. The size of the substrate presents a width of 23 mm, a length of 25 mm, and a thickness of 1.5 mm. Each channel sensing layer measures 4.3 × 4 mm. The width and spacing of the IDEs are 200 $\mu$m, and the heating circuit was designed with a spacing of 400 $\mu$m between the electrodes for uniform heat dissipation. The circuit design proposed in this work allows easy integration with plug-and-play connectors with simultaneous measurement of the four-channel sensors and common temperature control for the heating circuit through an negative temperature coefficient (NTC) surface mount device (SMD) thermistor (47 kΩ, reference NTCS0805E3 from the manufacturer Vishay).

### A. Graphite Deposition on PCB Sensor

A commercial spray composed of conductive graphite (CAS 7782-42-5) and isopropyl alcohol was purchased from Henkel (Bonderite L-Gp G Aerosolized Graphite) for application as a sensor film. A spray actuator valve, controlled automatically using a coreless digital servo (model DS3235sg) and an automatic linear stage actuator to move the spray deposition system from left to right, was employed to ensure that the same deposition process was applied to all IDE sensors. The graphite solution was sprayed at a distance of 10 cm from the sensor electrode, and five layers of the coating were applied, interrupted by a 10-s break. A short pause was taken between sprays to ensure that the solvent had completely evaporated. In addition, the deposited sensor layers were dried on a hot plate at 100 °C for 30 min under room environment conditions.

### B. Microgas Chamber Design and Manufacture

In order to increase gas detection current response and shorten response time, we designed a polydimethylsiloxane (PDMS) microchamber with a volume of 55 $\mu$L.

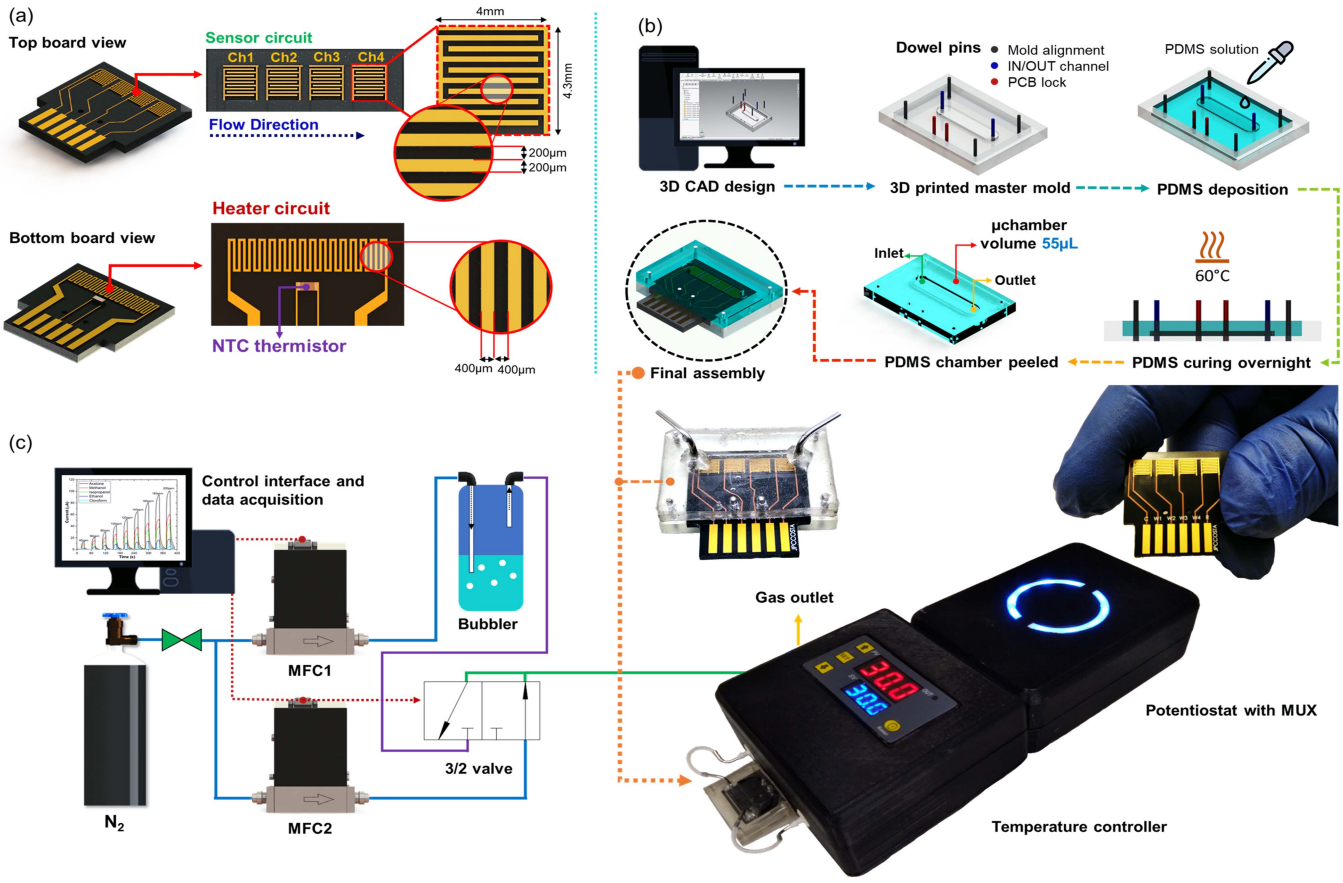


Fig. 1. (a) Developed 4-channel IDE sensor. (b) Concept with the manufacturing process for the PDMS microchamber. (c) Schematic of the experimental setup used in this work.

Several advantages arise when assembling the sensing system with a PDMS microchamber, for example, reagents and samples' amount reduction for analysis, low cost, precise control of experimental conditions, effective sealing to fluids and gases, and compatibility with different materials [30], [31], [32]. In addition, the combination of PDMS and current microfabrication technologies, such as soft lithography, micromilling, and print-and-peel, allows for the custom design of geometric microchannels and the integration and manipulation of multiple samples into a single device, which makes it an attractive candidate applied for the development of VOC sensors [33], [34].

To manufacture the PDMS microchamber, a patterning mold was designed in 3-D computer aided design (CAD) software (SolidWorks) and printed using a 3-D stereolithography (SLA) printer with a 405-nm clear UV resin. The mold was cured for 5 min with 405-nm UV light. To create the gas inlet and outlet channels, microchamber alignment, and locking it on the sensor board, dowel pins of 1 mm in diameter and 8 mm in length were placed in the respective location before applying the PDMS resin. PDMS solution was prepared by mixing the precursors Sylgard 184 silicone elastomer (Dow Corning) with a curing agent at a ratio of 10:1 by volume, followed by vacuum degassing for 30 min to remove all air bubbles in the mixture.

The PDMS mixture was poured into the 3-D-printed mold and cured overnight at 60 °C. After curing, the microchamber was removed from the mold. A stainless-steel elbow tube was added to the gas inlet and outlet connection and glued with epoxy on top of the microchamber to avoid any type of leakage. The connection to the gas injection system was made through a tube-to-tube fitting reduction connector (PMK220-210-1, Nordson Medical) with 1.6-mm internal diameter tubing. The microchamber manufacturing process is illustrated in Fig. 1(b).

### C. Instrumentation and Experimental Setup

The IDE sensor, developed and assembled with the microchamber, was connected to the measurement and control system via a 12-pin, gold-plated, double-edged connector (model 5650118-3, TE connectivity AMP connectors). The sensor was connected to a portable potentiostat designed by our group [35], modified with a multiplexer board (CD74HC4067), to simultaneously acquire the current of each sensor. Chronoamperometry was employed setting a fixed voltage of 2 V, and the response current was recorded simultaneously with an interval of 250 ms during 400 s. The developed heating system consists of a temperature controller model W3230 connected to the heating circuit at the bottom of the IDE sensor and its temperature is controlled by the NTC thermistor located in the center of the bottom board. The temperature for the heating circuit was set at 30 °C for all experiments. The flow system setup was strictly controlled using a Mass Flow MKS 1149 (maximum range of 200 sccm/$N_2$)

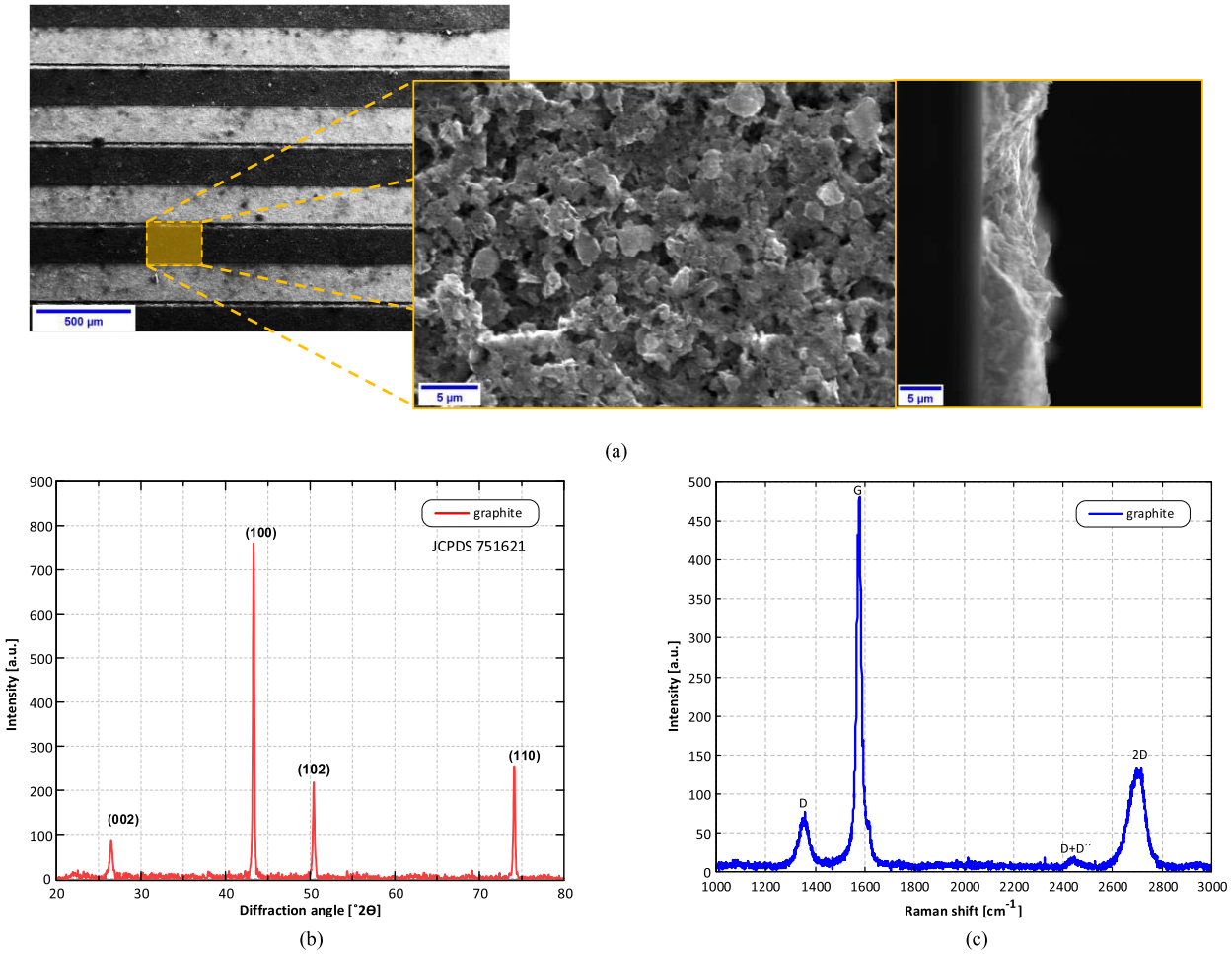


Fig. 2. (a) SEM image of the deposited graphite film on the IDE sensor, and respective (b) XRD pattern and (c) Raman spectra.

and nitrogen ($N_2$) cylinder ($O_2$ impurity $<$ 1 ppm), which was connected into two different lines, Line 1 and Line 2. Line 1 was used for $N_2$ transport, useful to remove undesirable gases, and Line 2 to assist VOCs' vapor transport [36]. VOC gases were then injected into the microchamber through the inlet port, and the sensor's change in current was observed as a function of exposure time. Target gases based on acetone, methanol, isopropanol, ethanol, and chloroform were introduced at different concentrations ranging from 40 to 200 ppm (step of 20 ppm) to evaluate the sensitivity and selectivity of the developed gas sensors. The concentration of the target gases was estimated according to de Araújo et al. [36]. Gas exposure was set as flowing for 15 s, considered as the VOC gas into the microchamber, and, for the following 30 s, only $N_2$ into the microchamber, with a total extent of 45 s. It was considered as a rise time, the time required for a sensor to reach 90% of the maximum response under exposure to the targeted gas, and recovery time as the one required for a sensor to reach 90% of the original baseline current upon removal of test gas [37]. Fig. 1(c) illustrates the experimental setup employed in this work.

### D. Characterization

Morphology of the deposited graphite film was investigated with a field emission scanning electron microscope (FE SEM) SEM JEOL 6510 operating at 20 kV. X-ray diffraction (XRD) measurements were carried out using Cu K$\alpha$ radiation (Rigaku diffractometer, model D/Max-2500PC) in a $2\theta$ range from 20° to 70°, with a step of 0.02° at a scanning speed of 2°min$^{-1}$. Micro-Raman spectra were recorded using the iHR550 spectrometer (Horiba Jobin-Yvon) equipped with a charge-coupled device detector and an argon-ion laser (Melles Griot) operating at 514.5 nm with a maximum power of 200 mW and a fiber microscope.

## IV. Results and Discussion

### A. Structure and Morphology Characterization

Fig. 2(a) shows the FE-SEM images of the film deposited on the IDE sensor. As can be seen, the spray deposition method allows a better uniformity of the graphite particles on the IDE sensor. A magnified view of the selected area of the sensor reveals that the graphite is composed of random plates arranged on its surface, with a certain porosity that offers better absorption and adsorption of the target gases. The cross-sectional image shows the compaction of the graphite particles, resulting in a thickness of approximately 6 $\mu$m, which was observed for all sensors.

Fig. 2(b) shows XRD patterns of graphite films deposited on IDE sensors. As can be seen, all XRD patterns are well in agreement with hexagonal graphite structures with $P63/mmc$ space groups in accordance with Joint Committee on Powder

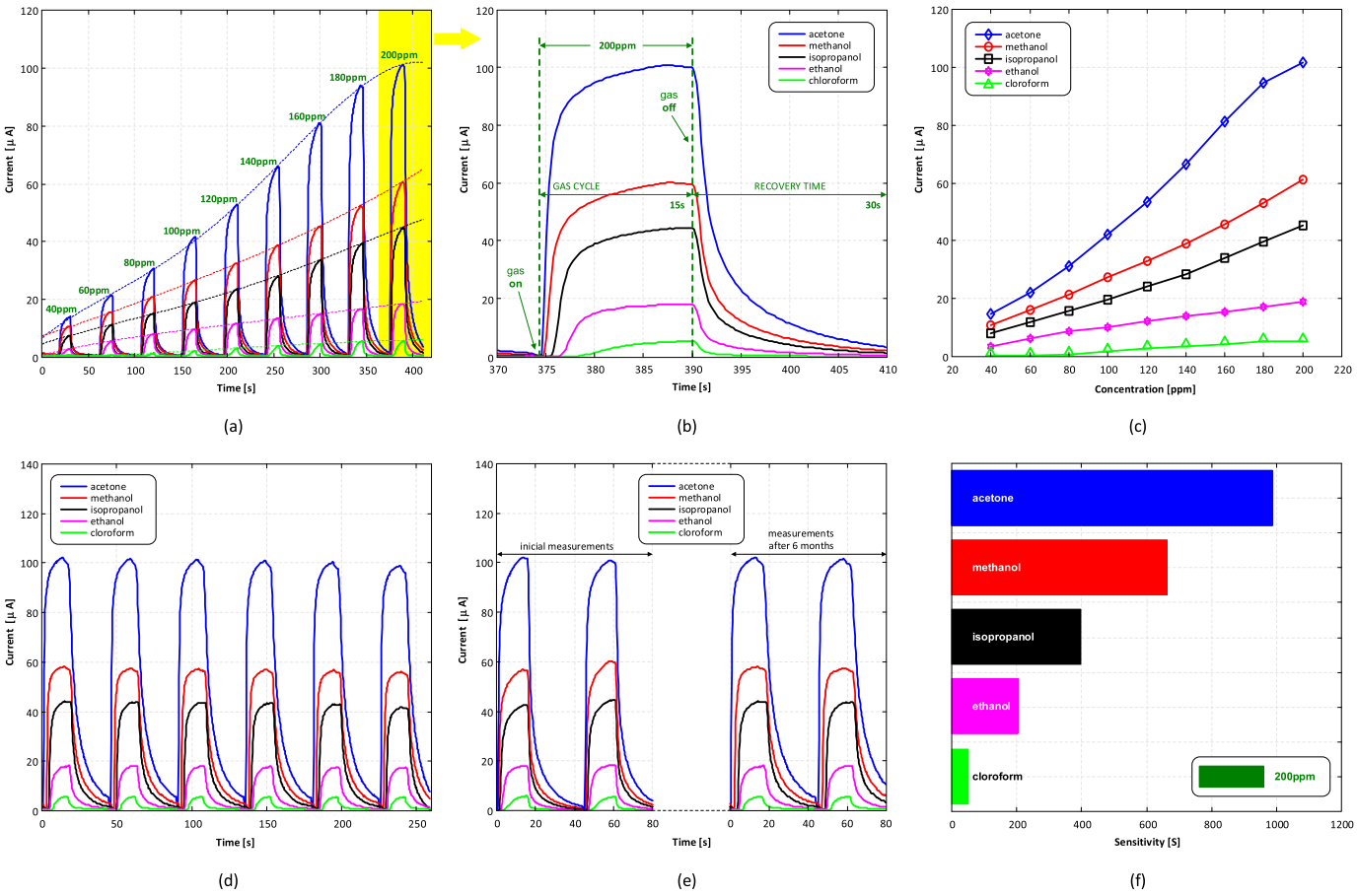


Fig. 3. Calibration curve for (a) all gases showing the current response pattern ($n = 4$). (b) Sensor sensitivity at 200 ppm. (c) Sensor response for all gases at different ppm concentrations. (d) Reproducibility test performed for all sensors at a 200-ppm cycle. (e) Long-term stability test performed after six months for all sensors at a 200-ppm cycle. (f) Sensor sensitivity at 200 ppm with a 15-s gas cycle and 30 s recovering under $N_2$.

Diffraction Standards (JCPDS) no. 751621 [38], [39]. A well-defined peak indicates a high degree of crystallinity at long range and a layered distribution of $sp^2$ carbon atoms.

The peaks located at 26.44°, 43.32°, and 50.44° correspond to the reflection of (002), (100), and (102) of the graphite structure, respectively.

A Raman spectrum of the graphite film deposited on the IDE sensor is shown in Fig. 2(c). As can be seen, tree bands dominate the Raman spectrum (1580, 1350, and 2700 $cm^{-1}$). The band located at 1580 $cm^{-1}$, known as the *G*-band, is formed by Raman scattering of in-plane longitudinal and transverse optical phonons in the center of the Brillouin zone [40], [41], [42]. The band located at 1350 $cm^{-1}$, known as the *D*-band, corresponds to the breathing mode of graphite, graphene, or graphene oxide structures due to transversal optical phonons at the Brillouin zone corner K [29], [30]. This band is generated in response to defects such as structural disorder, vacancies, strain, and edge effects. Additionally, a band was detected at 2700 $cm^{-1}$, which was associated with the double resonance of the *D*-band, known as the 2-D band [43].

### *B. Electrical Characterization and Sensing Response*

Electrical characterizations as a function of concentration for the five studied VOCs, operating at room temperature and under an applied voltage of 2 V, are shown in Fig. 3(a). Each peak represents a current response to a gas concentration increase in a 20-ppm step throughout time. In all measurements, intervals were established as a 15-s "gas on" condition, where there is a target VOC flow, and a 30-s "gas off" condition, in which the target VOC flow is ceased and an $N_2$ injection starts to assist the sensor's return to an equilibrium condition. In the first condition, a current increase in function of time is referred to as rising time, whereas in the latter, a current decrease in function of time is ascribed as recovery time. A rise time behavior observed for all VOCs is expected, since it is related to the number of molecules that can interact with available electrons on graphite's surface [36]. In Fig. 3(b), VOCs' rise and recovery curves for a 200-ppm concentration are highlighted, in which one can note a clear distinction of current values for each VOC studied. Such distinction indicates that each VOC's adsorption/desorption mechanism can be related to specific electronic levels on graphite's surface, that is, electronic affinity to each type of molecule results in a particular current variation. Given that, Fig. 3(c) presents a calibration curve as a function of concentration (ppm) for each VOC, based on four sensors studied in this experiment. Noteworthy that even at low concentrations (40 ppm), there is a clear distinct response among the gases. At higher concentrations, all VOCs

TABLE I
FITTING CURVE DATA FOR (2) FOR DIFFERENT VOCS

| Gas [200ppm cycle] | Rise sequence | | Recovery sequence | |
|---|---|---|---|---|
| | τ[s] | $R^2$[%] | τ[s] | $R^2$[%] |
| *Acetone* | 0.92 | 99.11 | 2.62 | 98.99 |
| *Methanol* | 1.36 | 98.71 | 2.26 | 98.72 |
| *Isopropanol* | 1.56 | 99.17 | 2.12 | 98.71 |
| *Ethanol* | 2.06 | 99.47 | 1.69 | 98.23 |
| *Chloroform* | 5.96 | 99.48 | 1.20 | 98.73 |

presented high current values, especially acetone. However, for chloroform, this behavior was noted only in a range of 80–180 ppm, also demonstrating a clear saturation trend above 180 ppm. Fig. 3(d) and (e) shows the reproducibility and long-term stability test performed at a 200-ppm cycle for all gases after six months from the initial experiments, respectively. Fig. 3(f) depicts the sensor's sensitivity for each VOC at a 200-ppm cycle. An analysis of Fig. 3(b) indicates that the measured current for adsorption and recovery rate cycles for different compounds can be modeled using exponential equations and time constants [44]. The equations obtained through the fitting of the experimental data are given by

$$I(t) = I_{\Delta}.e^{-\left(\frac{t-t_0}{\tau}\right)} + I_0 \tag{2}$$

where $\tau$ [s] is the time constant previously mentioned and $I_{\Delta}$ [A] is the difference in current with respect to the initial current $I_0$ [A]. Table I presents that the rise time for all the gases remained below 6 s, being symptomatic of the prompt response of the sensor. The recovery time constant was also evaluated and for all the gases it remained below 3 s.

By comparison to other studies based on $sp^2$ materials, as shown in Table II, our sensors demonstrated outstanding performance for the most responsive gas (acetone) and significantly even for chloroform, which showed the lowest response in terms of current gain. Furthermore, our sensors presented faster response and recovery times for the relatively low gas concentration value. Due to our devices' multiplexed structure, detection method, and ability to detect different types of VOC gases, this work offers wide application possibilities in scenarios where prompt detection of toxic gases is essential.

### C. Gas Sensor Mechanism

The mechanism underlying the detection of the organic molecules is related to the adsorption of these molecules onto the graphite surface and the interaction with the pi electrons of graphite, there being a transfer of charge to the organic molecule, and as a consequence, the formation of defects leading to polarization at short and medium ranges. The intensity and the observed reversibility of the sensor response can be directly associated with the differences in the electronic structure of the molecules resulting in physical interaction at the graphite surface. These interactions are driven by particular relations characterizing the molecules themselves, the morphology, and the grain boundary between the graphite particles. The graphite film is composed of a large number of

TABLE II
COMPARISON OF DIFFERENT VOC GAS SENSOR DEVICES OPERATING AT ROOM TEMPERATURE WITH THE RESPECTIVE SENSITIVITY, RISE/RECOVERY, AND DETECTION METHODS TO THE SENSOR DEVELOPED IN THIS WORK

| Sensing Material | Analyte/ ppm | Sensitivity | Rise/ Recovery(s) | Detection method | Ref |
|---|---|---|---|---|---|
| Graphite | Acetone/200 | 985 | 0.92/2.62 | [A] | This work |
| | Methanol/200 | 662 | 1.36/2.26 | | |
| | IPA/200 | 395 | 1.56/2.12 | | |
| | Ethanol/200 | 206 | 2.06/1.69 | | |
| | Chloroform/200 | 53 | 5.96/1.20 | | |
| MXene | Acetone/0.08 | 124 | 22.41/30.84 | [Hz] | [44] |
| | Methanol/0.08 | 93 | 20.83/7.84 | | |
| | Ethanol/0.08 | 76 | 21.58/5.05 | | |
| | IPA/0.08 | 20 | 25.92/4.28 | | |
| MWCNT/ PEG | Acetone/100 | 6% | 110/152 | [Ω] | [45] |
| | IPA/100 | 7% | | | |
| | Ethanol/100 | 8% | | | |
| *GO/GF* | IPA/1500 | 16% | 60/60 | [Ω] | [46] |
| | Ethanol/1500 | 8% | | | |
| | Methanol/1500 | 7% | | | |
| *RGO* | Chloroform/800 | 4.3% | 180/180 | [Ω] | [47] |

grains where charges build up in the grain boundary enhancing the molecule–graphite interaction. This process is also favored by the ability of the analytes to diffuse through the graphite film contributing to different sensing responses.

The interaction of organic molecules (gases)/graphite can be then analyzed in terms of the lamellar structure of graphite with sigma-type bonds forming a plane, perpendicularly pi-type bonds (electrons loosely bound to the graphite structure), and the polarity of the gases. In this way, chloroform has no electronic structure for electron transfer, so it adsorbs to a lesser extent. On the other hand, acetone has oxygen with pi electrons that can interact more strongly with the graphite structure, producing a more marked electronic defect. In addition, methanol, isopropanol, and ethanol gases can intercalate between the lamellae, forming a graphite/graphene heterostructure [48]. These defects and the polarities of the molecules interspersed in the graphite structure can change its bandgap and make it more conductive. The experimental results obtained confirmed that the different molecules, with different levels of polarization, led to a variation in conductivity, according to Fig. 3(a).

## V. CONCLUSION

In this article, we report a multiplexed gas sensor with graphite as the sensing material at room temperature. Among the advantages of the proposed sensor in this work is the ease of fabrication of IDE sensors using PCB technology, the reduction of gas detection time through the design and fabrication of a microchamber in PDMS, and the deposition of the sensor material by the spray method. The sensing material was demonstrated to be able to easily discriminate specific organic VOC gases such as acetone, methanol, isopropanol, ethanol, and chloroform, at room temperature. The gas sensor mechanism suggests that the increase in detection can be attributed to the polarity of the gas molecules that are adsorbing onto the surface of the graphite. Furthermore, sensors showed high stability and reproducibility after six months of the initial experiments. These preliminary findings could lead

to the development of a highly sensitive, low-cost multiple detection gas sensor for toxic organic compounds.

## REFERENCES


[1] S. Pandey, "Highly sensitive and selective chemiresistor gas/vapor sensors based on polyaniline nanocomposite: A comprehensive review," *J. Sci. Adv. Mater. Devices*, vol. 1, no. 4, pp. 431–453, Dec. 2016, doi: 10.1016/J.JSAMD.2016.10.005.

[2] A. Alagh, F. E. Annanouch, P. Umek, C. Bittencourt, J. F. Colomer, and E. Llobet, "An ultrasensitive room-temperature HS gas sensor based on 3D assembly of CuO decorated WS nanomaterial," *IEEE Sensors J.*, vol. 21, no. 19, pp. 21212–21220, Oct. 2021, doi: 10.1109/JSEN.2021.3103925.

[3] Z. Yuan, F. Yang, F. Meng, K. Zuo, and J. Li, "Research of low-power MEMS-based micro hotplates gas sensor: A review," *IEEE Sensors J.*, vol. 21, no. 17, pp. 18368–18380, Sep. 2021, doi: 10.1109/JSEN.2021.3088440.

[4] P. Bhattacharyya and D. Acharyya, "Impact of device configurations on sensing performance of $WS_2$-based gas sensors: A review," *IEEE Sensors J.*, vol. 21, no. 20, pp. 22414–22425, Oct. 2021, doi: 10.1109/JSEN.2021.3104615.

[5] J. T. Gurusamy et al., "MEMS based hydrogen sensing with parts-per-billion resolution," *Sens. Actuators B, Chem.*, vol. 281, pp. 335–342, Feb. 2019, doi: 10.1016/J.SNB.2018.07.118.

[6] L. Dong et al., "A characterization of the performance of gas sensor based on heater in different gas flow rate environments," *IEEE Trans. Ind. Informat.*, vol. 16, no. 10, pp. 6281–6290, Oct. 2020, doi: 10.1109/TII.2019.2963683.

[7] D. Zhang, Z. Yang, P. Li, M. Pang, and Q. Xue, "Flexible self-powered high-performance ammonia sensor based on Au-decorated $MoSe_2$ nanoflowers driven by single layer $MoS_2$-flake piezoelectric nanogenerator," *Nano Energy*, vol. 65, Nov. 2019, Art. no. 103974, doi: 10.1016/J.NANOEN.2019.103974.

[8] D. Wang, D. Zhang, Y. Yang, Q. Mi, J. Zhang, and L. Yu, "Multifunctional latex/polytetrafluoroethylene-based triboelectric nanogenerator for self-powered organ-like MXene/metal–organic framework-derived CuO nanohybrid ammonia sensor," *ACS Nano*, vol. 15, no. 2, pp. 2911–2919, Feb. 2021, doi: 10.1021/ACSNANO.0C09015.

[9] D. Wang et al., "Ethylene chlorotrifluoroethylene/hydrogel-based liquid-solid triboelectric nanogenerator driven self-powered MXene-based sensor system for marine environmental monitoring," *Nano Energy*, vol. 100, Sep. 2022, Art. no. 107509, doi: 10.1016/J.NANOEN.2022.107509.

[10] A. Sohrabi, P. M. Shaibani, M. H. Zarifi, M. Daneshmand, and T. Thundat, "A novel technique for rapid vapor detection using swelling polymer covered microstrip ring resonator," in *IEEE MTT-S Int. Microw. Symp. Dig.*, Jun. 2014, pp. 1–4, doi: 10.1109/MWSYM.2014.6848306.

[11] A. Mirzaei, S. G. Leonardi, and G. Neri, "Detection of hazardous volatile organic compounds (VOCs) by metal oxide nanostructures-based gas sensors: A review," *Ceram. Int.*, vol. 42, no. 14, pp. 15119–15141, Nov. 2016, doi: 10.1016/J.CERAMINT.2016.06.145.

[12] K. K. Sappati and S. Bhadra, "Printed acoustic sensor for low concentration volatile organic compound monitoring," *IEEE Sensors J.*, vol. 21, no. 8, pp. 9808–9818, Apr. 2021, doi: 10.1109/JSEN.2021.3056002.

[13] A. K. Pathak and C. Viphavakit, "VOC biomarker monitoring for diabetes through exhaled breath using Ag/P-$TiO_2$ composite plasmonic sensor," *IEEE Sensors J.*, vol. 21, no. 20, pp. 22631–22637, Oct. 2021, doi: 10.1109/JSEN.2021.3104766.

[14] Z. Chen, Y. Zheng, K. Chen, H. Li, and J. Jian, "Concentration estimator of mixed VOC gases using sensor array with neural networks and decision tree learning," *IEEE Sensors J.*, vol. 17, no. 6, pp. 1884–1892, Mar. 2017, doi: 10.1109/JSEN.2017.2653400.

[15] T. C. Miller, S. D. Morgera, S. E. Saddow, A. Takshi, and M. Palm, "Electronic nose with detection method for alcohol, acetone, and carbon monoxide in coronavirus disease 2019 breath simulation model," *IEEE Sensors J.*, vol. 21, no. 14, pp. 15935–15943, Jul. 2021, doi: 10.1109/JSEN.2021.3076102.

[16] D. Wang, D. Zhang, and Q. Mi, "A high-performance room temperature benzene gas sensor based on $CoTiO_3$ covered $TiO_2$ nanospheres decorated with Pd nanoparticles," *Sens. Actuators B, Chem.*, vol. 350, Jan. 2022, Art. no. 130830, doi: 10.1016/J.SNB.2021.130830.

[17] M. V. Nikolic, V. Milovanovic, Z. Z. Vasiljevic, and Z. Stamenkovic, "Semiconductor gas sensors: Materials, technology, design, and application," *Sensors*, vol. 20, no. 22, pp. 1–31, Nov. 2020, doi: 10.3390/S20226694.

[18] M. Tomić, M. Šetka, L. Vojkåvka, and S. Vallejos, "VOCs sensing by metal oxides, conductive polymers, and carbon-based materials," *Nanomaterials*, vol. 11, no. 2, pp. 1–34, Feb. 2021, doi: 10.3390/NANO11020552.

[19] P. Dariyal, S. Sharma, G. S. Chauhan, B. P. Singh, and S. R. Dhakate, "Recent trends in gas sensing via carbon nanomaterials: Outlook and challenges," *Nanosc. Adv.*, vol. 3, no. 23, pp. 6514–6544, Nov. 2021, doi: 10.1039/D1NA00707F.

[20] L. Sacco, S. Forel, I. Florea, and C.-S. Cojocaru, "Ultra-sensitive $NO_2$ gas sensors based on single-wall carbon nanotube field effect transistors: Monitoring from ppm to ppb level," *Carbon*, vol. 157, pp. 631–639, Feb. 2020, doi: 10.1016/J.CARBON.2019.10.073.

[21] N. Mohammad Yusof, S. Ibrahim, and S. Rozali, "Advances on graphene-based gas sensors for acetone detection based on its physical and chemical attributes," *J. Mater. Res.*, vol. 37, no. 2, pp. 405–423, Jan. 2022, doi: 10.1557/S43578-021-00456-3.

[22] N. R. Tanguy et al., "Flexible, robust, and high-performance gas sensors based on lignocellulosic nanofibrils," *Carbohydrate Polym.*, vol. 278, Feb. 2022, Art. no. 118920, doi: 10.1016/J.CARBPOL.2021.118920.

[23] S. R. Anjum, V. N. Narwade, K. A. Bogle, and R. S. Khairnar, "Graphite doped hydroxyapatite nanoceramic: Selective alcohol sensor," *Nano-Structures Nano-Objects*, vol. 14, pp. 98–105, Apr. 2018, doi: 10.1016/J.NANOSO.2018.01.010.

[24] X. Yu, C. Cheng, S. Feng, X. Jia, and H. Song, "Porous $\alpha$-$Fe_2O_3$ nanorods@graphite nanocomposites with improved high temperature gas sensitive properties," *J. Alloys Compounds*, vol. 784, pp. 1261–1269, May 2019, doi: 10.1016/J.JALLCOM.2019.01.099.

[25] D. S. Dasdan, "Poly (phenyl sulfone)/graphite composite as a robust low-cost, comb-type interdigited sensor for detection of organic solvent vapors," *J. Polym. Res.*, vol. 28, no. 4, pp. 1–9, Apr. 2021, doi: 10.1007/S10965-021-02489-Y.

[26] D. Wang et al., "Rotating triboelectric-electromagnetic nanogenerator driven by tires for self-powered MXene-based flexible wearable electronics," *Chem. Eng. J.*, vol. 446, Oct. 2022, Art. no. 136914, doi: 10.1016/J.CEJ.2022.136914.

[27] R. N. Chua, Y. W. Hau, C. M. Tiew, and W. L. Hau, "Investigation of attention deficit/hyperactivity disorder assessment using electro interstitial scan based on chronoamperometry technique," *IEEE Access*, vol. 7, pp. 144679–144690, 2019, doi: 10.1109/ACCESS.2019.2938095.

[28] S. S. Ghoreishizadeh, S. Carrara, and G. De Micheli, "Circuit design for human metabolites biochip," in *Proc. IEEE Biomed. Circuits Syst. Conf. (BioCAS)*, Nov. 2011, pp. 460–463, doi: 10.1109/BIOCAS.2011.6107827.

[29] V. M. Bright, E. S. Kolesar, and N. T. Hauschild, "Investigation of the sensitivity, selectivity, and reversibility of the chemically-sensitive field-effect transistor (CHEMFET) to detect NO/sub 2/, C/sub 3/H/sub 9/PO/sub 3/, and BF/sub 3/," in *Proc. Nat. Aerosp. Electron. Conf. (NAECON)*, Dec. 2002, pp. 342–349, doi: 10.1109/NAECON.1994.332987.

[30] G. G. Morbioli, N. C. Speller, and A. M. Stockton, "A practical guide to rapid-prototyping of PDMS-based microfluidic devices: A tutorial," *Analytica Chim. Acta*, vol. 1135, pp. 150–174, Oct. 2020, doi: 10.1016/J.ACA.2020.09.013.

[31] I. Miranda et al., "Properties and applications of PDMS for biomedical engineering: A review," *J. Funct. Biomaterials*, vol. 13, no. 1, p. 2, Dec. 2021, doi: 10.3390/JFB13010002.

[32] V. F. Cardoso et al., "Polymer-based acoustic streaming for improving mixing and reaction times in microfluidic applications," *RSC Adv.*, vol. 4, no. 9, pp. 4292–4300, Dec. 2013, doi: 10.1039/C3RA46420B.

[33] D.-B. Luo, Y.-X. Duan, Y. He, and B. Gao, "A novel DC microplasma sensor constructed in a cavity PDMS chamber with needle electrodes for fast detection of methanol-containing spirit," *Sci. Rep.*, vol. 4, no. 1, pp. 1–9, Dec. 2014, doi: 10.1038/SREP07451.

[34] V. Faustino, S. O. Catarino, R. Lima, and G. Minas, "Biomedical microfluidic devices by using low-cost fabrication techniques: A review," *J. Biomechanics*, vol. 49, no. 11, pp. 2280–2292, Jul. 2016, doi: 10.1016/J.JBIOMECH.2015.11.031.

[35] J. P. de Campos da Costa, W. B. Bastos, P. I. da Costa, M. A. Zaghete, E. Longo, and J. P. Carmo, "Portable laboratory platform with electrochemical biosensors for immunodiagnostic of hepatitis C virus," *IEEE Sensors J.*, vol. 19, no. 22, pp. 10701–10709, Nov. 2019, doi: 10.1109/JSEN.2019.2930957.

[36] E. P. de Araújo, C. A. Amorim, A. N. Arantes, and A. J. Chiquito, "A label-free acetone based $SnO_2$ nanowire network sensor at room temperature," *Appl. Phys. A, Solids Surf.*, vol. 128, no. 5, pp. 1–8, May 2022, doi: 10.1007/S00339-022-05540-X.

[37] T. Bhowmick et al., "Multilayered and chemiresistive thin and thick film gas sensors for air quality monitoring," *Multilayer Thin Films*, vol. 1, pp. 127–166, Jan. 2020, doi: 10.5772/INTECHOPEN.89710.
[38] Z. Q. Li, C. J. Lu, Z. P. Xia, Y. Zhou, and Z. Luo, "X-ray diffraction patterns of graphite and turbostratic carbon," *Carbon*, vol. 45, no. 8, pp. 1686–1695, Jul. 2007, doi: 10.1016/J.CARBON.2007.03.038.
[39] W.-J. Lee, Y.-T. Wu, Y.-W. Liao, and Y.-T. Liu, "Graphite felt modified by atomic layer deposition with $TiO_2$ nanocoating exhibits superhydrophilicity, low charge-transform resistance, and high electrochemical activity," *Nanomaterials*, vol. 10, no. 9, p. 1710, Aug. 2020, doi: 10.3390/NANO10091710.
[40] J.-B. Wu, M.-L. Lin, X. Cong, H.-N. Liu, and P.-H. Tan, "Raman spectroscopy of graphene-based materials and its applications in related devices," *Chem. Soc. Rev.*, vol. 47, no. 5, pp. 1822–1873, 2018, doi: 10.1039/C6CS00915H.
[41] V. Zólyomi, J. Koltai, and J. Kürti, "Resonance Raman spectroscopy of graphite and graphene," *Phys. Status Solidi B*, vol. 248, no. 11, pp. 2435–2444, Nov. 2011, doi: 10.1002/PSSB.201100295.
[42] J. P. de Campos da Costa et al., "A scalable electron beam irradiation platform applied for allotropic carbon transformation," *Carbon*, vol. 174, pp. 567–580, Apr. 2021, doi: 10.1016/J.CARBON.2020.11.054.
[43] S. Roscher, R. Hoffmann, and O. Ambacher, "Determination of the graphene-graphite ratio of graphene powder by Raman 2D band symmetry analysis," *Anal. Methods*, vol. 11, no. 9, pp. 1180–1191, Mar. 2019, doi: 10.1039/C8AY02619J.
[44] K. K. Kazemi et al., "Low-profile planar antenna sensor based on $Ti_3C_2T_x$ MXene membrane for VOC and humidity monitoring," *Adv. Mater. Interface*, vol. 9, no. 13, May 2022, Art. no. 2102411, doi: 10.1002/ADMI.202102411.
[45] Z. Liu, T. Yang, Y. Dong, and X. Wang, "A room temperature VOCs gas sensor based on a layer by layer multi-walled carbon nanotubes/polyethylene glycol composite," *Sensors*, vol. 18, no. 9, p. 3113, Sep. 2018, doi: 10.3390/S18093113.
[46] S. Aslam, T. H. Bokhari, T. Anwar, U. Khan, A. Nairan, and K. Khan, "Graphene oxide coated graphene foam based chemical sensor," *Mater. Lett.*, vol. 235, pp. 66–70, Jan. 2019, doi: 10.1016/J.MATLET.2018.09.164.
[47] A. Midya, S. Mukherjee, S. Roy, S. Santra, N. Manna, and S. K. Ray, "Selective chloroform sensor using thiol functionalized reduced graphene oxide at room temperature," *Mater. Res. Exp.*, vol. 5, no. 2, Feb. 2018, Art. no. 025604, doi: 10.1088/2053-1591/AAA67B.
[48] E. Schröder, "Methanol adsorption on graphene," *J. Nanomaterials*, vol. 2013, pp. 1–6, Jan. 2013, doi: 10.1155/2013/871706.

**João Paulo de Campos da Costa** (Member, IEEE) was born in Ribeirão Preto, Brazil, in 1991. He received the B.Eng. degree in electrical engineering from the Universidade de Araraquara (UNIARA), Araraquara, Brazil, in 2015, and the M.Sc. degree from the University of São Paulo (USP), São Paulo, São Carlos, Brazil, in 2018, where he is currently pursuing the Ph.D. degree in electrical engineering with the Telecommunications and Optics Group.

He developed multifunctional materials for piezoelectric nanogenerators, gas sensors, varistors, and solar cell applications at the Centro de Desenvolvimento de Materiais Funcionais (CDMF), São Paulo. He is a member of the CDMF/Fundação de Amparo à Pesquisa do Estado de São Paulo (FAPESP) Research Group, São Paulo. His scientific interests include sensors, biosensors, and electron beam-enhanced nanomaterials.

**Leonélio Cichetto Junior** received the B.S. degree in physics and the M.Sc. and Ph.D. degrees in condensed matter physics in the area of superconducting thin films and pulsed laser deposition (PLD) from the Federal University of São Calos (UFSCar), São Paulo, São Carlos, Brazil, in 2006, 2009, and 2013, respectively.

He is a Researcher at São Paulo State University (UNESP), São Paulo, and Universität Jaume, Castellón de la Plana, Spain, and a member of the NanOLaB and Centro de Desenvolvimento de Materiais Funcionais (CDMF)/Fundação de Amparo à Pesquisa do Estado de São Paulo (FAPESP) Research Group, São Paulo. His scientific interests include electron transport in thin-film nanostructures and materials irradiation by femtosecond laser and electron beam.

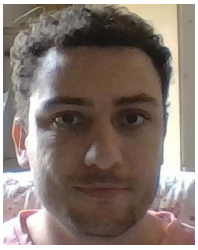

**Estácio Paiva de Araújo** was born in Ponta Grossa, Brazil, in 1988. He received the M.Sc. degree in science of materials physics from the Federal University of Uberlândia, Uberlândia, Brazil, in 2017. He is currently pursuing the Ph.D. degree in applied physics with the Federal University of São Carlos, São Paulo, Brazil.

His research interests include electronic transport phenomena, nanotechnology, and biosensors.

**Adryelle do Nascimento Arantes** received the degree in medical physics from the Federal University of Uberlândia (UFU), Uberlândia, Brazil, in 2017, and the M.Sc. degree in applied physics from the Federal University of São Carlos (UFSCar), São Paulo, São Carlos, Brazil, in 2021.

She was a member of the NanOLaB Research Group, São Paulo. Her research interests include electronic transport phenomena, nanotechnology, and biosensors.

**Elson Longo** received the B.S. degree in chemistry from the Institute of Chemistry, São Paulo State University (UNESP), Araraquara, Brazil, in 1969, and the M.Sc. and Ph.D. degrees in physics–chemistry from the Physics Institute, University of São Paulo (USP), São Paulo, São Carlos, Brazil, in 1975 and 1984, respectively.

He is an Emeritus Professor and the Chairperson of the Chemistry Department at UFSCar, São Carlos, SP, Brazil. He maintains strong connections with national and international research universities in Spain, Portugal, France, the USA, and Italy. He is also the Director of the Center for the Development of Functional Materials [CDMF/Fundação de Amparo à Pesquisa do Estado de São Paulo (FAPESP)], a member of the International Academy of Ceramics (World Academy of Ceramics), Academy of Sciences of the State of São Paulo (ACIESP), and the Brazilian Academy of Sciences.

**Adenilson José Chiquito** received the B.S. degree in physics and the M.Sc. and Ph.D. degrees in condensed matter physics from the Federal University of São Carlos (UFSCar), São Paulo, São Carlos, Brazil, in 1994, 1997, and 2001, respectively.

He held a postdoctoral position in physics at the University of São Paulo (USP), São Paulo, working with electron transport in semiconductor nanostructures under high magnetic fields. He is currently a Professor and the Head of the NanOLaB Laboratory at the Physics Department, UFSCar. He has experience in electron transport in low-dimensional systems, optical and electrical properties of semiconductors, and scientific instrumentation.

**João Paulo Carmo** was born in Maia, Portugal, in 1970. He received the Ph.D. degree in industrial electronics from the University of Minho, Guimarães, Portugal, in 2007. His Ph.D. thesis was on RF transceivers for integration in microsystems to be used in wireless sensor network applications.

He is currently an Associate Professor at the University of São Paulo (USP), São Paulo, Brazil, where he is involved in research on micro/nanofabrication technologies for optical and mixed-mode/RF microsystems, solid-state integrated sensors, microactuators, and micro/nanodevices for use in biomedical and industrial applications. He is also the Vice-Director of the Group of Metamaterials Microwaves and Optics (GMeta), USP.